J. Fluid Mech. (2004), *vol.* 519, *pp.* 55–80.
DOI: 10.1017/S0022112004001028 Printed in the United Kingdom

Erosion and deposition of particles on a bed sheared by a viscous flow

By F. CHARRU, H. MOUILLERON AND O. EIFF

IMFT, Allée C. Soula, 31400 Toulouse, France

(Received 5 August 2003 and in revised form 30 June 2004)

Experiments are reported on the dynamics of a bed of particles sheared by a viscous Couette flow in an annular channel, with emphasis on the distributions of particle velocities, durations and lengths of the small saltation flights, and surface density of the moving particles. The velocity distributions are shown to decay approximately exponentially, with mean value, U_p, equal to $0.1\,\gamma d$, where γ is the shear rate and d is the particle diameter. The duration of the flights does not depend on the shear rate, and is equal to 15 times the settling time d/V_S, where V_S is the Stokes settling velocity. Starting from an initially loosely packed bed, the surface density of the moving particles, N_p, was observed to decrease slowly over several days, unlike their velocity which remains constant with time. This decay is related to the increase of the threshold shear rate for particle motion, and corresponds to rearrangement of the particles near the bed surface (armouring). When the stationary state is reached, N_p depends linearly on the shear rate, so that the particle flow rate, $Q_p = N_p U_p$, is a quadratic function of the shear rate. Two theoretical models are proposed to account for these observations. In the first one, the erosion and deposition rates are modelled using the two hydrodynamic time scales: the inverse shear rate γ^{-1} for the erosion rate, and the settling time d/V_S for the deposition rate. This model accounts for the linear dependence of N_p on the shear rate. The second model was developed to capture the slow decrease of N_p, by considering the trapping of moving particles into troughs of the bed. This trapping model does recover the main features observed experimentally, although the characteristic time for the decrease of N_p still remains too short. Our observations are, finally, compared to existing numerical and experimental studies on turbulent flows.

1. Introduction

Erosion and deposition of particles by a shear flow are phenomena involved in numerous industrial processes, such as oil extraction, and in the natural environment, such as sediment transport by water, thus spanning a wide range of particle Reynolds numbers. Although much work has been devoted to the subject for more than a century, no general theory exists. In particular, as noted by the ASCE Task Committee on Flow and Transport over Dunes (2002), the problem of predicting the suspended-load and bed-load flow rates, which are the main practical quantities of interest, is not satisfactorily solved yet for turbulent flows. The presumably simpler situation of viscous flows is not understood either, even four decades after Bagnold's incitement to study 'laminar flows' (Bagnold 1966).

From the experimental point of view, the existing data are mostly for turbulent flows and are widely scattered, even for nearly uniform sediment size. This is true

for the threshold for particle motion as a function of the particle Reynolds number (Buffington & Montgomery 1997), i.e. the well-known Shields curve, as well as for the particle flow rate (Bagnold 1966; Wiberg & Smith 1989). The observed scatter in these laws, as often stated, is certainly due to the difficulty of controlling and determining the flow and particle parameters, such as the turbulent flow near the bed, the size, shape and roughness of the particles. To some extent the scatter is also due to the difficulty of unambiguously defining the quantities of interest. Less studied are the particle flow variations that arise from the long-term evolution of the bed at the particle scale, in particular bed armouring. Such long-term evolution is still poorly understood and is in particular believed to concern mainly beds of non-uniform sized particles (Chin, Melville & Raudkivi 1994). The lack of understanding is at least partly due to the technical difficulty associated with traditional flume experiments, which are always limited in length, and as a consequence the basic physical phenomena involved have received little attention. Notwithstanding the intrinsic interest of understanding such long-term evolution, it should be noted that even if the intent is to only study the stationary situation, one needs to know the time scales that are necessary to reach this state.

From the modelling point of view, the pioneering papers by Einstein (1950) and Bagnold (1956) in the field of hydraulics, and, in the context of viscous resuspension, that of Leighton & Acrivos (1986), have yielded the basic concepts to model the bed-load flow rate. The semi-empirical laws they proposed have been improved since, mainly from investigations of the saltating motion of individual particles (Bagnold 1973; van Rijn 1984; Engelund & Fredsoe 1976; Wiberg & Smith 1989; Sekine & Kikkawa 1992) and also from experiments (Fernandez Luque & van Beek 1976). These laws are widely used in hydraulic engineering for transport predictions (Raudkivi 1998), and also to account for ripple and dune formation under steady and oscillating flows (Richards 1980; Blondeaux 1990), tidal currents (Blondeaux 2001), or viscous flows (Charru & Mouilleron-Arnould 2002). However, these laws are not firmly rooted in undisputable hydrodynamic models, and they consequently fail in some situations. In particular, it is recognized that the laws based on Bagnold's original concepts are not accurate for bottom shear stresses close to the threshold of particle motion. Moreover, the above models ignore the problem of bed compaction, and to our knowledge there are again no models predicting the time scales of this phenomenon.

Not only are the bed-load flow-rate laws not clearly determined and understood yet, but they also concern an integrated quantity: the bed load, i.e. particle flow rate, is the product of the mean velocity of the particles and their surface density. This surface density in turn results from the two opposite processes of erosion and deposition. Fundamental progress in the field requires these quantities (i.e. the mean particle velocity and surface density, as well as the erosion and deposition rates) to be determined, which in turn requires the description of the motion of individual particles. Such a description has already been given by Meland & Normann (1966) and Francis (1973) for a single particle on a bed of fixed particles. Fernandez Luque & van Beek (1976) report the mean velocity, saltation lengths and surface density of moving particles for water flows. However, little is known on the distributions of these quantities, and viscous flows have not been investigated yet.

In the light of the complexities and the current level of understanding, this paper investigates the simple and prototypical situation of a plane horizontal bed of particles sheared by a viscous Couette flow $U(y)$, with no ripple formation. The first objective is to re-examine the threshold for particle motion, and above this threshold, to determine

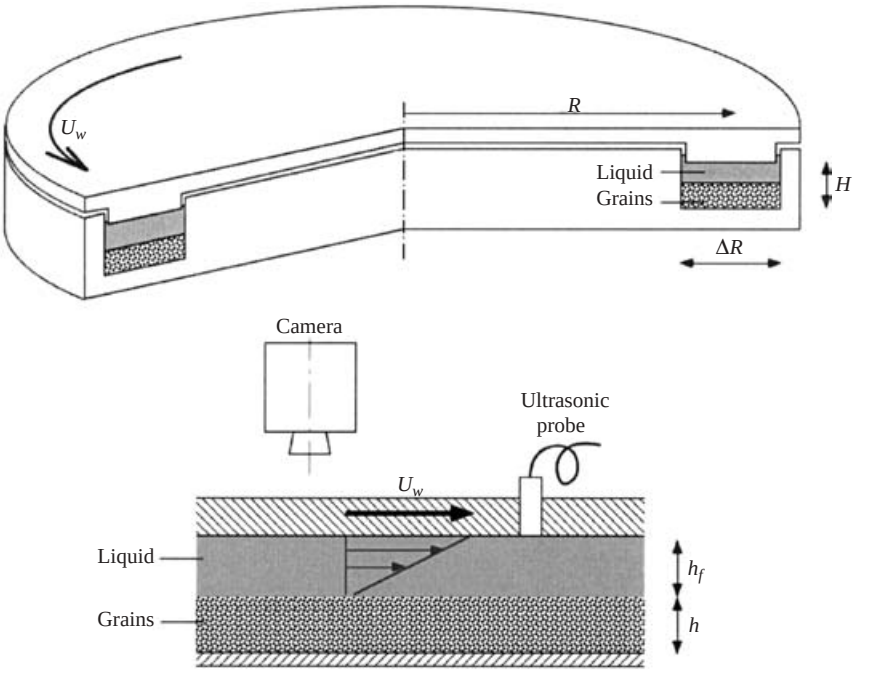

FIGURE 1. Sketch of the annular channel. $R = 200\,\text{mm}$, $\Delta R = 40\,\text{mm}$, $H = 16\,\text{mm}$, $h_f \approx 7\,\text{mm}$.

the velocity distributions and surface density of the moving particles. This is done by taking into account the long-term evolution (up to five days) of a loosely packed bed towards a saturated 'armoured' bed. The second objective is to propose two models to account for the underlying physical processes: a 'dynamic' model for the erosion and deposition processes, and a 'kinematic' model for the long-term evolution of the particle flow rate.

The paper is organized as follows: The experimental set-up based on an annular geometry is described in § 2 and the results are given in § 3. The two models are developed in § 4. The final section is devoted to a discussion of the results in connection with previous studies.

2. Experimental set-up

Experiments have been performed in an annular Plexiglas channel, of mean radius $R = 200\,\text{mm}$ (figure 1). The advantage of a closed channel is that it avoids the problems associated with the supply of fluid and particles to ensure stationary and homogeneous flow conditions. Moreover, long-term evolution can be studied, in contrast with open-ended channels. The width and depth of the channel are $\Delta R = 40\,\text{mm}$ and $H = 16\,\text{mm}$, respectively. The rotation of the upper plate, whose velocity at the mean radius is denoted U_w, drags the fluid, which in turn drags the particle bed. For the results presented here, the fluid is silicon oil (density $\rho_f = 950\,\text{kg m}^{-3}$, viscosity $\mu = 19.5 \times 10^{-3}\,\text{Pa s}$ at $20\,^{\circ}\text{C}$), with a typical thickness $h_f \approx 7\,\text{mm}$. Particles are spherical acrylic beads (density $\rho_p = 1180\,\text{kg m}^{-3}$). They have been sieved in order to reduce the size dispersion: histogramms obtained from a granulometer gave a mean diameter $d = 0.58\,\text{mm}$ with a standard deviation of about 0.1 mm. A fixed fraction of them (5%) were dyed for easier identification as discussed later in § 3.3.

The main fluid flow is azimuthal and close to plane Couette flow, $U_f = \gamma y$, where $\gamma = U_w/h_f$ is the shear rate. However, there is also a small secondary flow due to centrifugal forces, directed outwards in the upper half of the fluid layer and inwards in the lower half. The radial velocity W_f can be estimated by balancing the radial pressure gradient due to centrifugal forces, of order $\rho_f U_w^2/R$, with the viscous resistance, of order $\mu W_f/h_f^2$, giving $W_f/U_w \sim Re\, h_f/R$, where

$$Re = \frac{\rho_f U_w h_f}{\mu} \tag{1}$$

is the channel Reynolds number. This small radial velocity induces a radial bottom shear stress, of order $\mu W_f/h_f$, which slowly drags the particles to the inner wall. From the above estimates, the ratio of the radial to the main azimuthal shear stress can be written as

$$\frac{\tau_r}{\tau_a} = c\ Re\ \frac{h_f}{R}, \tag{2}$$

where c is a constant depending on the aspect ratio of the channel. The above estimates have been confirmed by numerical simulations of the flow in an annular channel with smooth walls (Mouilleron-Arnould 2002). These simulations show that for $Re < 200$, (i) the azimuthal velocity U_f departs from Couette flow by less than 10% in the middle half of the width of the channel, and (ii) the constant c in (2) is 0.06 for the aspect ratio $\Delta R/h_f = 40/7$, and varies very little with the latter. Thus, for the maximum channel Reynolds number examined ($Re_{max} = 43$), the maximum radial velocity W_f is less than 3% of the upper plate velocity, and the predicted radial bottom shear stress is 9% of the azimuthal component. The radial bottom shear stress is responsible for a slow drift of the particles towards the inner wall of the channel, eventually resulting in a radial inclination of the bed surface. For the results presented here, the maximum difference in the bed (or fluid) thickness across the width of the channel remained less than 1 mm, i.e. about two particle diameters.

The particle motion depends on the relative magnitude of the hydrodynamic force acting on it, of order $\mu\gamma d^2$, and its apparent weight, of order $(\rho_p - \rho_f)gd^3$. The ratio of these two forces defines the Shields number,

$$\theta = \frac{\mu\gamma}{(\rho_p - \rho_f)gd}. \tag{3}$$

The particle motion also depends on the relative magnitude of inertial and viscous stresses, i.e. on the particle Reynolds number,

$$Re_p = \frac{\rho_f \gamma d^2}{\mu}. \tag{4}$$

For the experiments to be presented, the dimensionless parameters ranged from zero up to $Re = 43$, $\theta = 0.24$ and $Re_p = 0.30$. Above these upper bounds the secondary flow due to centrifugal effects is no longer negligible.

The bed height along the mean radius R was measured using an ultrasonic probe, mounted flush with the lower surface of the upper plate as shown in figure 1. The diameter of the ultrasonic beam is about 3 mm. The bed surface is visualized from above with an interlaced colour CCD camera, with resolution 768×576 pixels, and a sampling frequency of 25 Hz. The field of view was $13 \times 10\,\mathrm{mm}^2$ centred on the mean radius of the channel and aligned with the longitudinal direction. A particle diameter therefore corresponds to 33 pixels in the longitudinal direction. Due to the high concentration of the moving particles and the weak contrast between the moving

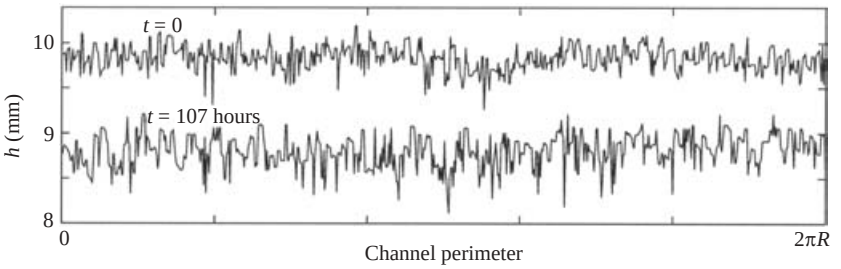

FIGURE 2. Bed thickness as measured by the ultrasonic probe, at the onset of motion and 107 hours later, for $\theta = 0.17$ ($\gamma = 11\,s^{-1}$).

particles and the underlying bed, the use of an automatic tracking procedure was not feasible. Thus, the particles were manually tracked from frame to frame. Their centre was determined with the aid of the image-processing software Optimas©, with an accuracy of one pixel corresponding to about $0.03d$.

Due to the near-matching of the optical indexes of the fluid and the particles, dyed particles located three or four particle diameters below the bed surface could be identified, allowing the thickness of the moving layer to be estimated. Close to the threshold of particle motion, $\theta = 0.04$, only a few particles move at the bed surface. For the highest Shields number studied, $\theta = 0.24$, the moving layer is about two diameters thick, but small displacements are visible down to four particles diameters below the bed surface. Of course the vertical positions of the particles cannot be obtained from the upper view of the bed. A detailed study of the moving layer and of the particle and fluid velocities within this moving layer has been undertaken (Mouilleron-Arnould 2002) and will be published elsewhere.

3. Experimental results

In this experimental section we first address the temporal bed-thickness evolution of an initially loosely packed bed under steady shear conditions (§ 3.1). We then turn to the motion of individual particles (§ 3.2), followed by the surface density of the moving particles (§ 3.3). Finally, on the basis of these measurements we give the Shields-number dependence of the flow rate on a compacted bed (§ 3.4).

3.1. *Bed-thickness evolution*

The first step preceding any measurement was to prepare a flat bed, achieved by rotating the upper plate sufficiently fast in order to resuspend the whole bed and then quickly stopping the upper plate. The particles settle, and form a loosely packed flat bed after a few minutes. It should be noted that the Stokes settling velocity of a particle is $V_S = (\rho_p - \rho_f)gd^2/18\mu \approx 2.2\,\mathrm{mm\,s^{-1}}$ and the characteristic settling time is $d/V_S \approx 0.27$ s. A typical profile of the initial bed surface ($t = 0$), as measured by the ultrasonic probe, is shown on the upper trace of figure 2. It can be seen that the residual fluctuations of the bed surface or thickness are about one particle diameter, as expected.

Particles begin to move for Shields numbers above a threshold, defined as $\theta_{t,0}$, of 0.04. For a constant Shields number above this threshold, the mean bed thickness is observed to decrease slowly with time. This is illustrated in figure 2, which shows the bed thickness at the initial time ($h \approx 9.8\,\mathrm{mm}$), and after four days ($h \approx 8.8\,\mathrm{mm}$). This bed subsidence, of about two particle diameters, is expected to be caused by

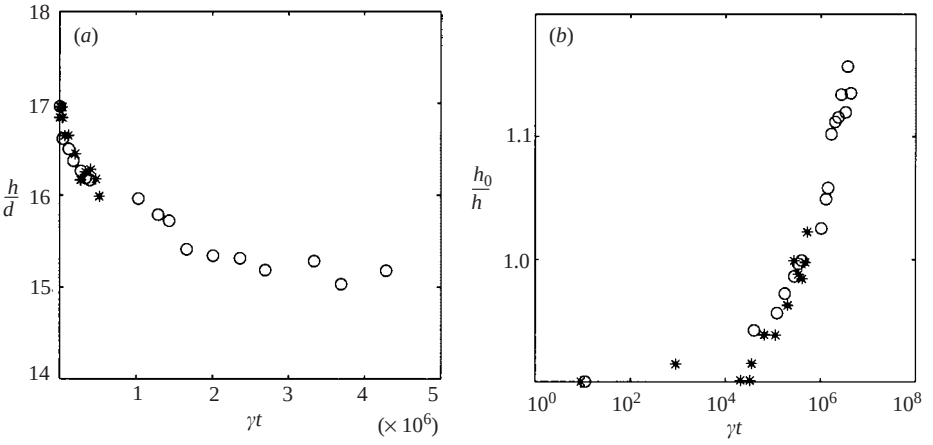

FIGURE 3. (*a*) Temporal evolution of the mean bed thickness h/d, for $\theta = 0.14$ (*) and 0.17 (○) ($\gamma = 9$ and $11\,\mathrm{s}^{-1}$, respectively); (*b*) temporal evolution (log scale) of h_0/h where h_0 is the initial mean bed thickness.

two phenomena: first, the local rearrangements of the particles which lead to an increase of the compactness, and second, the slow drift of the particles towards the inner wall due to the centrifugal secondary flow. The relative importance of these two phenomena can be determined by measuring the radial profile of the bed. Such measurements have been performed with the help of a cathetometer (the ultrasonic probe could not be translated radially), but the accuracy was not sufficient for a firm conclusion to be drawn on this basis. However, as will be seen, all other evidence points towards an increase in compactness.

The temporal evolution of the mean bed thickness is shown in figure 3(*a*) for two Shields numbers. For the higher one ($\theta = 0.17$) the thickness variation is faster, and it can be seen that the two temporal evolutions collapse when plotted versus the dimensionless time γt. The thickness varies strongly — by two particle diameters — until $\gamma t \approx 2 \times 10^6$ corresponding to several hours. For later times, the variation is much weaker — about a tenth of a diameter — and dominated by fluctuations due to measurements errors. Figure 3(*b*) displays the same temporal evolution in terms of the inverse of the bed thickness, h_0/h, where h_0 is the mean bed thickness at the onset of motion. It can be seen that for dimensionless times γt greater than 10^4 (i.e. after about 15 minutes), this ratio increases logarithmically with time. Such a logarithmic evolution is similar to that observed for the compaction of granular material shaken vertically, for which a phenomenological theory has been proposed (Kadanoff 1999), which is a first indication that the observed bed subsidence is due to compaction.

It should be noted that the subsidence of the bed surface, of about one millimetre, is not negligible compared to the fluid thickness, $h_f \approx 7\,\mathrm{mm}$. Thus, in order to keep the shear rate constant, the upper plate velocity has to be gradually increased, by about 15% during the course of the run. It should also be noted that, as can be seen in figure 2, no ripple formation was observed; indeed, ripples were observed to grow with water or low-viscosity oil, but they disappeared for a viscosity of about ten times that of water. This will be reported and discussed in a forthcoming paper.

3.2. *Motion of individual particles*

We present in this section a study of the motion of the individual particles, specifically their trajectories and velocities. These quantities have been evaluated for Shields

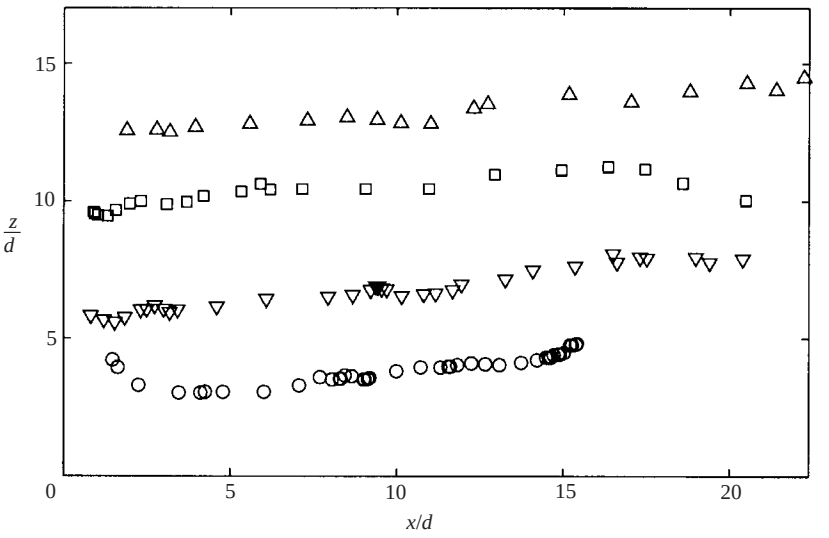

FIGURE 4. Four particle trajectories at nominal time $\gamma t = 10^3$ for $\theta = 0.24$ ($\gamma = 19\,\mathrm{s}^{-1}$). The flow is from left to right, and the time interval between two successive positions is 0.4 s.

numbers up to $\theta = 0.24$ and, in order to evaluate possible long transients effects, at nominal times $\gamma t = 10^3$, 10^4, 10^5 and 10^6, the latter time corresponding to two days.

Figure 4 displays four typical particle trajectories at the surface of the bed for $\theta = 0.24$, obtained from an image sequence of one minute taken 15 minutes after the beginning of the run. The motion appears irregular due to the bumps encountered by the moving particles over the other moving or fixed particles. For the shear-stress range studied (one to six times the threshold $\theta_{t,0} = 0.04$), the particles mainly roll over each other, with small 'flights' at a height of about one particle diameter above the bed. A particle may stop for a while in a small trough, and then start again, generally due to the impact of another particle or possibly due to the rearrangement of the particles around it. The trajectories reported in figure 4 correspond to 'fast' particles, i.e. particles crossing a significant part of the field of view during the image sequence. Many other particles were observed to experience small displacements, again likely to be related to the local re-arrangement of the microstructure of the bed.

Once the successive positions of the moving particles are recorded, their quasi-instantaneous velocity can be computed. Considering the particle positions at time intervals of 0.40 s (only one frame in ten was retained for velocity computations) and the camera resolution corresponding to 0.017 mm, the resolution of the velocity measurements is $0.042\,\mathrm{mm\,s}^{-1}$. In terms of the characteristic fluid velocity γd at a distance d above the bed, this cut-off corresponds to $0.006\,\gamma d$ for $\theta = 0.15$ and to $0.004\,\gamma d$ for $\theta = 0.24$. Figure 5 displays the temporal evolution of the longitudinal velocity component U of eight particles, tracked from their entrance to their exit of the field of view, for the same flow conditions as in figure 4. It can be seen that velocities exhibit large fluctuations between $U \approx 0$ and $U \approx 0.4\,\gamma d$. Velocities higher than $0.2\,\gamma d$ generally occur as isolated peaks. The fact that the velocity may become zero means that the particle stops and then starts again. The mean longitudinal particle velocity, defined as U_p, is about $0.10\,\gamma d$, or, in terms of the Stokes settling velocity, about $0.43\,V_S$.

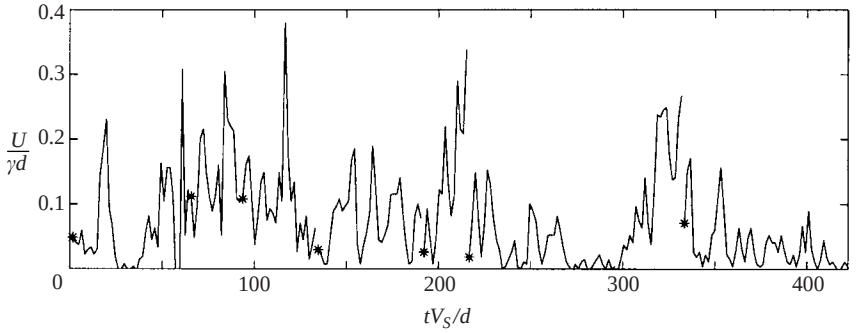

FIGURE 5. Time variation of the velocity of eight particles, at nominal time $\gamma t = 10^3$ for $\theta = 0.24$ ($\gamma = 19\,\mathrm{s}^{-1}$); each star corresponds to the beginning of the tracking of a new particle (the time scale has only a relative value).

In order to determine the long-term evolution of particle velocity and flights, just considering their mean value may be insufficient. More information can be gained from their distribution, i.e. their probability density functions (PDFs). Such PDFs have been determined for the particle velocities, for which several hundred measurements were available. For the duration and length of the flights, the number of measurements was at least one order of magnitude lower, which was not enough for obtaining converged PDFs, but enough for coarse histograms and estimates of the most probable values.

The velocity PDFs can be obtained by two different methods. The first or 'Eulerian' method consists in identifying all the moving particles between two successive frames, and then averaging over a suitable number of frames, until convergence is achieved. When the number of moving particles was too high (greater than about one hundred), only dyed particles were considered. This method requires a precise definition of a 'moving particle', taken as one with velocity greater than the cut-off velocity discussed earlier. The second or 'Lagrangian' method for determining the velocity PDFs considers the successive velocities of the same particles as they cross the field of the camera, at time intervals of 0.4 s, and then averaging over a suitable number of particles. Among these velocities, 10% to 20% are zero (i.e. less than the cut-off $0.042\,\mathrm{mm\,s}^{-1}$) and have been removed for the PDFs (they correspond to particles stopping). Figure 6 compares the PDFs obtained by the two methods, for the same flow conditions as in figure 4. The PDF obtained with the Eulerian method here corresponds to an average over 85 frames, each frame showing 5 to 12 dyed moving particles. The PDF obtained with the Lagrangian method corresponds to 227 velocities from 8 tracked particles. It can be seen that both methods lead essentially to the same PDF. In particular, the mean velocities are very close, $0.090\,\gamma d$ and $0.087\,\gamma d$ for the Eulerian and Lagrangian methods, respectively. This implies that no bias was introduced by selecting a sample of moving particles in the Lagrangian method. Since the Lagrangian method was more time efficient it was used for the following results and figures, with about 250 to 700 velocities measured by tracking 6 to 12 particles. Physically both methods reveals that the PDF decreases monotically to zero, approximately obeying the following exponential law:

$$P(U) = \frac{1}{U_p} \mathrm{e}^{-U/U_p} \quad \text{with} \quad \frac{U_p}{\gamma d} = 0.10. \tag{5}$$

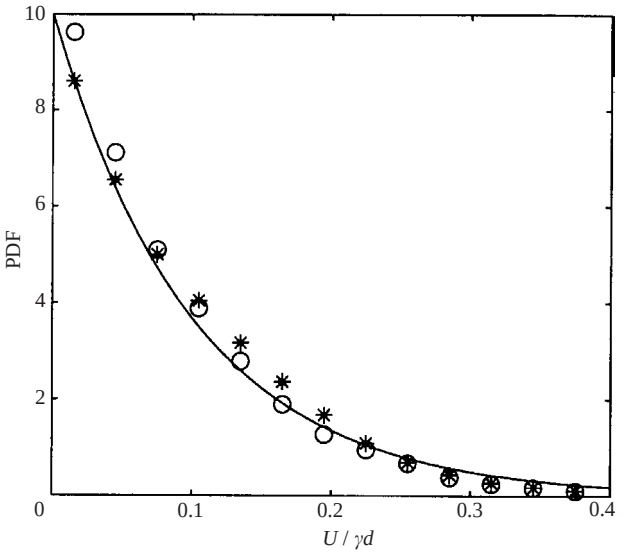

FIGURE 6. PDF of particle longitudinal velocity U at nominal time $\gamma t = 10^3$ for $\theta = 0.24$ ($\gamma = 19\,\mathrm{s}^{-1}$): *, Eulerian method; ○, Lagrangian method. Solid line: exponential distribution given by equation (5).

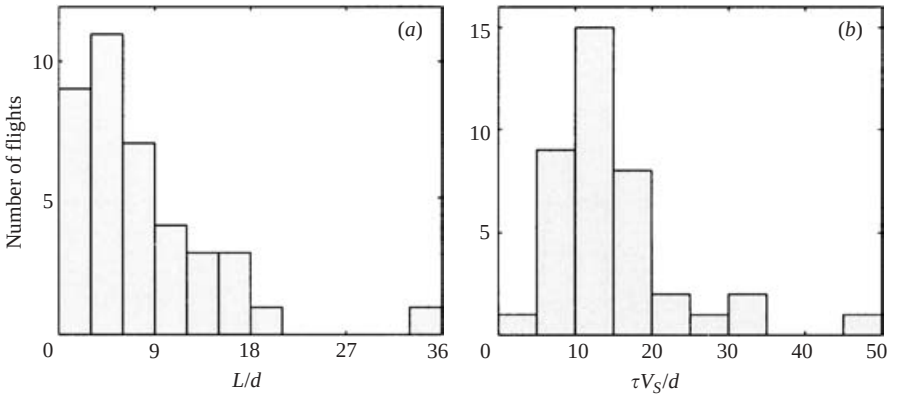

FIGURE 7. Histograms of (*a*) length and (*b*) duration of the particle flights, at nominal time $\gamma t = 10^3$ for $\theta = 0.24$ ($\gamma = 19\,\mathrm{s}^{-1}$).

The flight lengths L and flights durations τ of the particles have been determined by tracking the particles and their stop and start times. As mentioned before, the number of measurements was not enough for obtaining converged PDFs. Nevertheless, sample histograms are shown in figure 7. The distribution of the flight lengths (figure 7*a*) is strongly skewed towards long lengths and exhibits a peak at $L/d \approx 5$. However, this peak is not well-defined due to the coarse resolution and its closeness to zero. The distribution of the flight durations (figure 7*b*), on the other hand, is more symmetric and exhibits a well-defined peak corresponding to the most probable flight duration, defined as τ_p. This duration is about 4 s, or, in terms of the Stokes settling time, about $15\,d/V_S$. Few flight durations exceed three times the most probable one.

Figure 8 displays the time evolution of the PDF of the velocity U, still for $\theta = 0.24$, at nominal times ranging from $\gamma t = 10^3$ to 10^6. The figure reveals that the PDFs

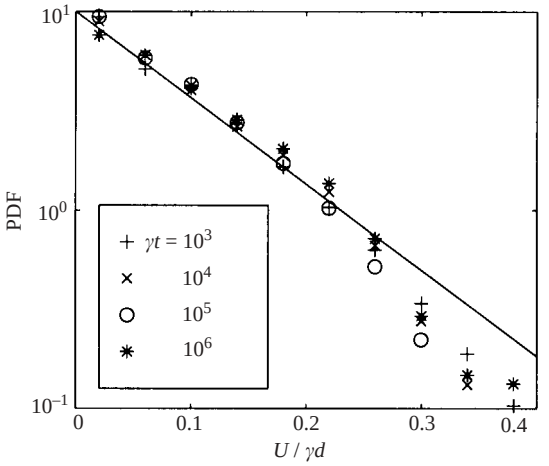

FIGURE 8. PDF of particle longitudinal velocity U at nominal times $\gamma t = 10^3$, 10^4, 10^5 and 10^6, for $\theta = 0.24$. Solid line: exponential distribution given by equation (5).

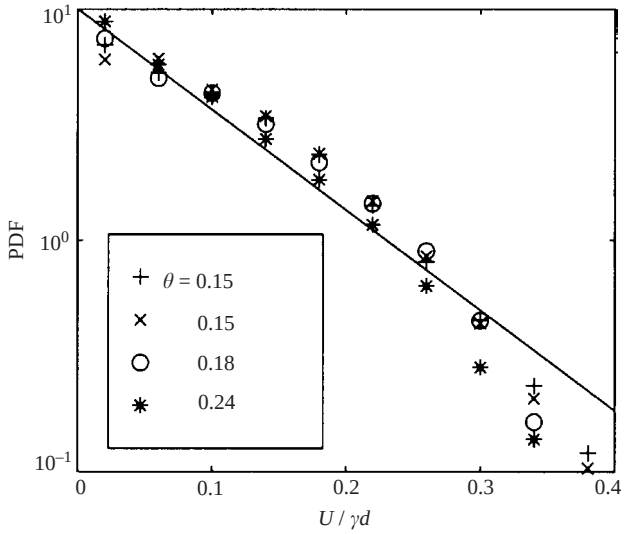

FIGURE 9. PDF of particle longitudinal velocity U for $\theta = 0.15$ (two runs), 0.18 and 0.24. Solid line: exponential distribution given by equation (5).

collapse rather well, implying that the velocity distribution is time-independent and approximately exponential as in equation (5), at least for velocities less than $0.25\,\gamma d$. It must be noted that the most probable flight length L_p and flight duration τ_p also do not appear to vary significantly with time, remaining close to $5d$ and $15\,d/V_S$, respectively.

The dependence of the velocity distribution on the Shields number has been explored for $\theta \leqslant 0.24$. First, for all θ, the PDFs of the velocities do not vary significantly with time as in figure 8 for $\theta = 0.24$. Secondly, as can be seen in figure 9, the PDFs are also independent of θ, at first order. However, closer inspection reveals that when θ increases from 0.15 to 0.24, there are slighly more small velocities and

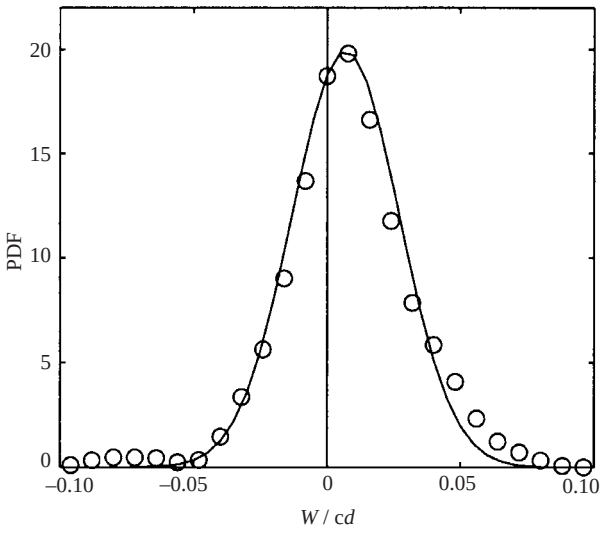

FIGURE 10. ○, PDF of particle transverse velocity W at nominal time $\gamma t = 10^3$ for $\theta = 0.24$ ($\gamma = 19\,\mathrm{s}^{-1}$). Solid line: Normal distribution with mean $W_p = 0.007\gamma d$ and standard deviation $\sigma_W = 0.02\gamma d$.

fewer high velocities, with the mean velocity decreasing from $0.10\,\gamma d$ to $0.09\,\gamma d$. It should also be noted that these results are only weakly sensitive to the cut-off at the low-velocity end of the PDFs. In particular, increasing the cut-off from the lowest measured velocity to twice this value increases the mean velocity by about 5% only, for all θ.

The Shields-number dependence of the duration and length of the flights has also been investigated. The most probable flight duration τ_p behaves like the velocity distribution: it does not vary significantly with time, for any θ, and it is also independent of θ, remaining close to $15\,d/V_S$. The flight length on the other hand increases with the shear rate, and is approximately given by $L_p \approx U_p \tau_p$.

As discussed in § 2, the curvature of the channel is responsible for a slow recirculating flow which induces a slow drift of the particles towards the inner wall of the channel. A typical PDF of the transverse velocity component W is shown in figure 10 for the highest Shields number studied, at the early stages of particle motion ($\gamma t = 10^3$). As expected, this PDF exhibits a non-zero mean value, $W_p = 0.007\gamma d = 0.07\,U_p$, which is in agreement with the numerical prediction of the radial bottom shear stress being 9% of the azimuthal component; the coefficient decreases for long times as the radial slope increases, and eventually vanishes when the transverse shear stress and sloping effects balance. The distribution of W_p is close to Gaussian, with standard deviation $\sigma_W \approx 0.03\,\gamma d$.

From the velocity distributions, the fluctuating kinetic energy of the particles contained in the random motion about the mean velocity, commonly referred to as the granular temperature $T = \langle (U - U_p)^2 + (W - W_p)^2 \rangle$, can be obtained. With the exponential distribution for U and the normal distribution for W, it is $T = U_p^2 + \sigma_W^2 \approx 0.011(\gamma d)^2$, where the contribution of the transverse velocity fluctuations is only 10%, i.e. the fluctuations are highly anisotropic. The scaling of the granular temperature with $(\gamma d)^2$ is a common result for dry granular flows (mainly from numerical simulations) when the intersticial fluid is ignored (Campbell 1990). For

such flows, the result $T \sim (\gamma d)^2$ can be inferred from dimensional analysis. However, this does not necessarily follow for viscous flows, for which there are other velocity scales than γd.

In summary, the following main conclusions can be drawn from the above observations. First, the velocity distributions decrease monotonically, in an approximately exponential manner. This distribution, when normalized with the characteristic velocity γd, is independent of time and Shields number, with mean velocity $U_p = 0.10\,\gamma d$. Second, the flight duration τ_p of the particles does not depend on time for fixed θ, and does not vary significantly either as θ is varied. Thus, at least for $\theta \leqslant 0.24$, the mean velocity to within 20%, and the mean duration and length of the flights to within 20%, are given by

$$\frac{U_p}{\gamma d} = 0.10, \quad \frac{\tau_p}{d/V_S} = 15, \quad \frac{L_p}{d} \approx \frac{U_p \tau_p}{d} = 27\,\theta. \tag{6}$$

3.3. *Surface density of moving particles, N_p*

In addition to considering the motion of individual particles, our objective was to determine the total number N_p of moving particles per unit area. This number can be determined by two differents methods. The first method is to count the number of particles which move between two successive frames, with the same definition of a 'moving particle', based on the spatial resolution, as in the Eulerian method of the previous section. The second method is to compute N_p from the number of particles crossing a transverse line of unit length per unit time, i.e. from the particle flow rate Q, with the relationship:

$$N_p = \frac{Q}{U_p}, \quad \text{where} \quad U_p = \int_0^\infty U\,P(U)\,\mathrm{d}U. \tag{7}$$

In this equation, the mean velocity U_p on the bed surface is defined from the probability density function $P(U)$ of the velocities, as determined in the previous section.† Note that the mean velocity U_p on the bed surface is different from the mean velocity of the particles crossing a transverse line. Indeed, the probability $P(U)\mathrm{d}U$ of finding a particle with velocity $U \pm \delta U/2$ on the bed surface is different from the probability $P'(U)\,\mathrm{d}U$ of measuring a velocity in the same range as a particle crosses a transverse line, the two probability densities being related by $P'(U) = (U/U_p)\,P(U)$.

The flow rate Q has been determined by counting the number of particles crossing a transverse line 1 cm long in the centre of the channel, where the fluid velocity is radially uniform. For high moving-particle concentrations, only the small fraction of dyed particles were counted, whereas for low concentrations all particles were considered. Using the mean particle velocity U_p obtained in the previous section, the number of moving particles can finally be defined from the measured particle flow rate Q as

$$N_p = \frac{Q}{U_p}, \quad \text{with} \quad U_p = 0.10\,\gamma d. \tag{8}$$

† The relationship (7), which is obvious when all particles have the same velocity, can be demonstrated, when the velocities are distributed, by considering the number δN_p of particles with velocity between U and $U + \delta U$ in a rectangle of length $U\delta t$ in the direction of the flow, and then integrating over all the velocities.

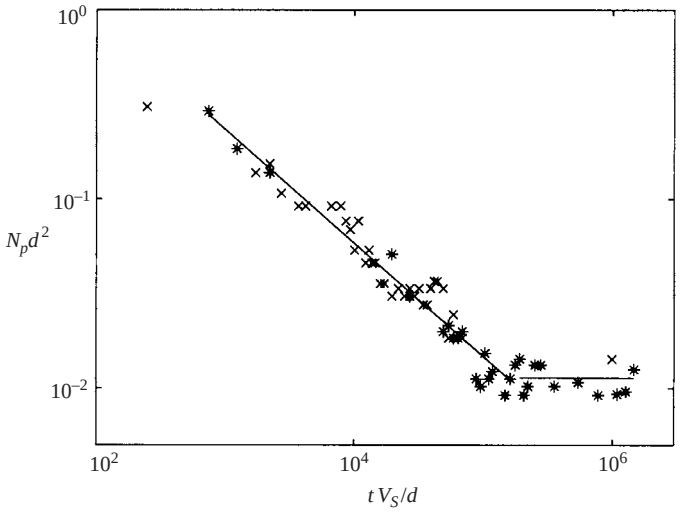

FIGURE 11. Temporal evolution of the surface density $N_p d^2$ of moving particles for $\theta = 0.15$ ($\gamma = 11\,\mathrm{s}^{-1}$). The symbols $*$ and $\times$ were determined using (8), and correspond to two different runs.

Both methods for the determination of N_p, the direct-counting method and equation (8), were found to give close results, as discussed below. However, the determination from the particle flow rate and equation (8) is more time efficient.

Figure 11 displays a typical temporal evolution of the dimensionless surface density $N_p d^2$, which represents the number of moving particles on the area d^2, for $\theta = 0.15$. N_p was determined from equation (8), each point corresponding to the crossing of a few tens of counted particles over a period spanning a few minutes. The two symbols correspond to two different runs which were measured several weeks apart, showing that the measurements are reproducible. In contrast with the particle velocity which was shown to remain constant with time, it appears that the surface density of moving particles decreases strongly over very long times, by more than one order of magnitude, and then reaches a constant or saturated value $N_{p,sat} d^2 \approx 0.01$. The decrease lasts for $t_{sat} \approx 7\,\mathrm{hours} \approx 10^5\, d/V_S$, and approximately follows the power law $N_p \sim t^{-\alpha}$ with $\alpha \approx 0.60$. Note that the saturation time t_{sat} is much longer than any hydrodynamic time scale, and is comparable with the time scale of the variation of the bed thickness.

Figure 12 compares, for $\theta = 0.24$, the two methods of determination of the surface density: the direct counting of the moving particles in the field of view of the camera, and the determination via the flow rate and equation (8). It appears that, as mentioned above, both methods lead to close results. However, for $\theta = 0.15$, the other Shields number for which both methods were employed, the comparison displayed a significant discrepancy, up to a factor of two. The explanation is probably that the number of moving particles is not uniform over the bed. One cause for this is that when a moving particle happens to be stopped by a little bump or trough, the following particles may accumulate against it and form a packet. This 'metastable packet' may then be swept away by the impact of an additional particle, and it then disperses. This phenomena seems to be more pronounced for small particle flow rates. The non-uniformity of the surface density also implies an intermittency of the flow rate Q. Thus the estimation of N_p or Q may be biased if the period of time over

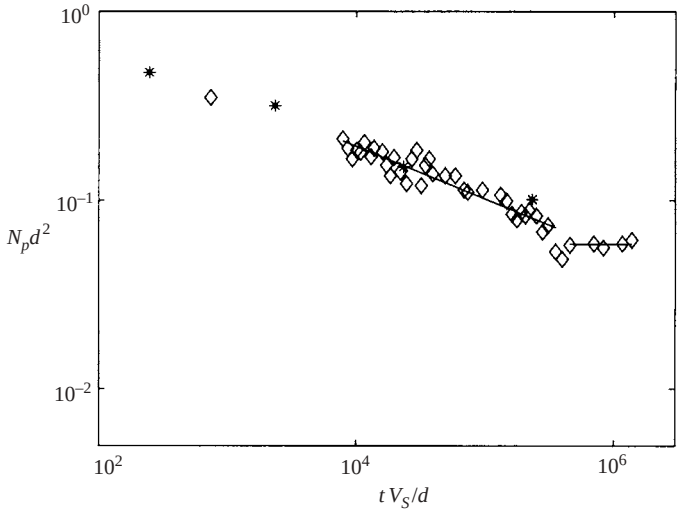

FIGURE 12. Time evolution of the surface density $N_p d^2$ of moving particles for $\theta = 0.24$ ($\gamma = 18\,\mathrm{s}^{-1}$): $*$, direct counting of the moving particles within the field of view of the camera; $\diamond$, determined using equation (8) with Q and U_p.

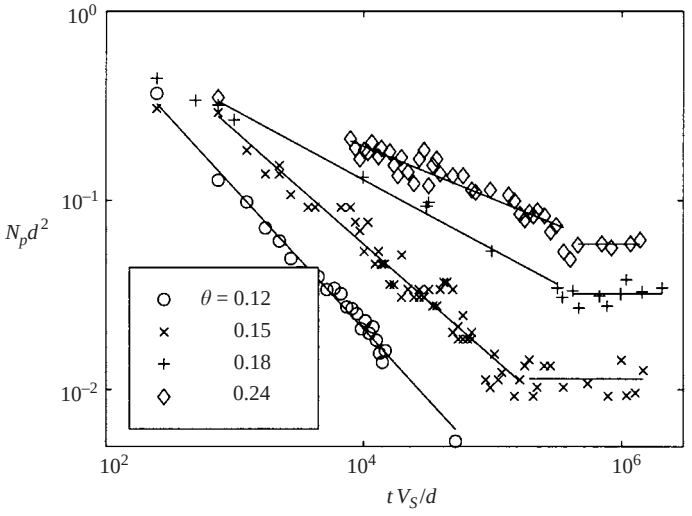

FIGURE 13. Time evolution of the number N_p of moving particles for Shields numbers $\theta = 0.12$, 0.15, 0.18 and 0.24.

which it is averaged is shorter than the characteristic time of the intermittency. From this point of view, we believe that the particle flow rate measurements, for which the averaging times ranged between one and ten minutes, are more reliable than the surface density measurements, which were averaged over a few tens of seconds only. The intermittency phenomena remains to be studied more precisely.

Figure 13 shows how the decrease of the surface density of moving particles changes with the Shields number. For $\theta = 0.24$, 0.18 and 0.15, it can be seen that the surface density decreases to a non-zero saturated value $N_{p,sat} d^2$ within a finite saturation time t_{sat}. For the lowest Shields number, $\theta = 0.12$, the saturated surface density is effectively

zero: the last point shown in the figure corresponds to ten particles crossing the field of view during two minutes; at time $\gamma t \approx 6 \times 10^5$ (not shown in the figure), there were only two over an interval of ten minutes. By extrapolating to zero the saturated particle flow rate, the minimum Shields number to obtain a non-zero saturated surface density (and flow rate) was found to be $\theta_{t,sat} = 0.12$, as discussed in more detail in the following section. As expected then, for θ in the range $\theta_{t,0} < \theta < \theta_{t,sat}$, the flow rate and surface density were observed to decrease to zero, and the particle motion was only transient.

The cause for the decrease of the number of moving particles is likely to be the rearrangement of the 'microstructure' of the particles near the bed surface. This is supported by the observation that some moving particles are seen to stop permanently, trapped in a trough between fixed grains, as evidenced, for example, in figure 4 for the lower particle. We were unable to demonstrate this rearrangement directly via the measurement of the bed roughness with the ultrasonic probe (see figure 2), which implies that the roughness changes occur on lengths smaller than the diameter of the probe beam, i.e. smaller than six particle diameters. The trapping model presented later, however, supports this type of bed surface evolution.

The rearrangement of the surface microstructure has an important macroscopic effect: it increases the threshold for particle motion, from the initial value $\theta_{t,0} = 0.04$, obtained for a settled bed after total resuspension, up to the saturated value $\theta_{t,sat} = 0.12$. This rise of the threshold Shields number corresponds to an 'armouring' of the bed. The saturation time t_{sat}, defined as the time needed for the saturated state to be reached, thus corresponds to an armouring time. The armouring process is irreversible. Indeed, we have observed that after stopping the flow for a while (a few minutes to a few hours) and starting it again, the threshold for particle motion is higher than the initial one, as long as the saturated value is not reached. Moreover, the particle flow rate does not exhibit any discontinuity: after the stop-restart sequence, it immediately recovers the value it had before it was stopped. This remains true even if the fluid flow is reversed. The saturated threshold is therefore likely to be independent of the way the bed was initially prepared, and is expected to be representative of some equilibrium state of the surface microstructure of the sheared bed. However, this equilibrium state and the corresponding threshold $\theta_{t,sat}$ may depend on the shape and on the dispersion of the size of the particles. This point will be re-addressed in the final section in relation to previous threshold measurements.

3.4. *Shields number dependence of the saturated flow rate*

The dependence of the particle flow rate on the bottom shear stress has received much attention in the literature due to its great practical importance. The semi-empirical laws that have been proposed all assume, at least implicitly, that the bed has reached an equilibrium state. In this section, we propose such a law for the viscous flow case. As noted in the previous section with regard to the results from figure 13, the number of moving particles, and thus the saturated flow rate $Q_{sat} = N_{p,sat} U_p$, increase with Shields number beyond the threshold $\theta_{t,sat}$. Figure 14 displays the experimental data for the dimensionless flow rate $Q_{sat}/(V_S/d^2)$ versus Shields number θ. These data are shown together with the parabolic fit

$$Q_{sat} \frac{d^2}{V_S} = 0.85\,\theta\,(\theta - \theta_{t,sat}) \quad \text{with} \quad \theta_{t,sat} = 0.12, \tag{9}$$

which is the only one which leads to good agreement with the experimental data. The saturated threshold $\theta_{t,sat} = 0.12$ first introduced in the previous section was determined

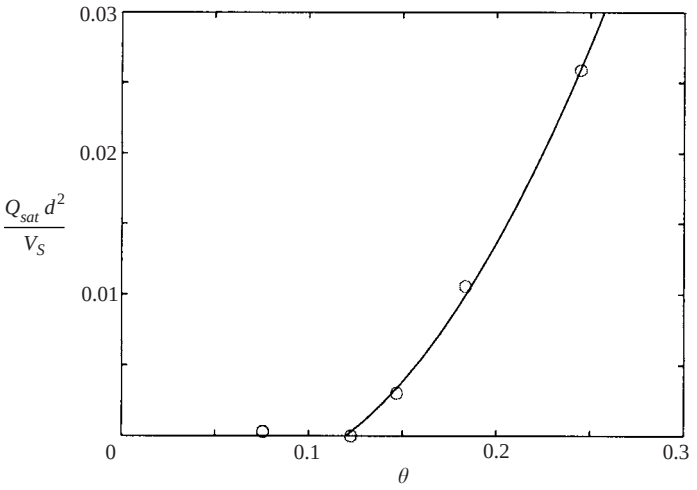

FIGURE 14. Saturated flow rate Q_{sat} versus Shields number θ: ○, experiments; solid line, parabolic fit given by equation (9).

from this parabolic fit. The dependence of $N_{p,sat}$ on the Shields number can now be obtained. Indeed, the particle flow rate Q_{sat} given by (9) being the product of U_p by $N_{p,sat}$, and $U_p = 0.10\,\gamma d = 1.8\,\theta\, V_S$ being linearly dependent on θ, implies that $N_{p,sat}$ varies according to the following linear law:

$$N_{p,sat} d^2 = 0.47\,(\theta - \theta_{t,sat}) \quad \text{with} \quad \theta_{t,sat} = 0.12. \tag{10}$$

3.5. *Summary of the experimental results*

The main observations reported can be summarized as follows:

1. For Shields numbers θ smaller than the threshold $\theta_{t,0} \approx 0.04$, particles do not move. This threshold is expected to depend on the way the bed is prepared (here, by sedimentation of the totally resuspended flow).

2. For $\theta > \theta_{t,0}$, some particles are set into motion. They experience flights whose duration $\tau_p \approx 15 d/V_S$ depends neither on time nor on the bottom shear stress. Their mean velocity is $U_p/(\gamma d) \approx 0.10$; it does not depend on time, and depends only slightly on the Shields number, decreasing by about 10% as the Shields number is doubled.

3. For $\theta_{t,0} < \theta < \theta_{t,sat}$, where $\theta_{t,sat} = 0.12$, the number N_p of moving particles per unit area decreases and eventually vanishes. The measurement of subsidence of the bed surface suggests this is due to the trapping of the moving particles in small troughs between fixed particles, and a reorganization of the surface microstructure of the bed (armouring).

4. For $\theta > \theta_{t,sat}$, the number N_p still decreases with time, but it eventually reaches a non-zero saturated value, such that $N_{p,sat} d^2 = 0.47(\theta - \theta_{t,sat})$. The saturated flow rate, $Q_{sat} = U_p N_{p,sat}$, is a quadratic function (9) of the shear rate.

5. The threshold $\theta_{t,sat}$ is expected to correspond to an asymptotic state of the surface microstructure of the bed, and is likely to be independent of the way the bed is prepared although dependent on the particle characteristics. This asymptotic state is reached after an armouring time t_{sat} of order $t_{sat} \approx 10^6/\gamma$. This time is very large compared to the hydrodynamic time scales $1/\gamma$ or d/V_S.

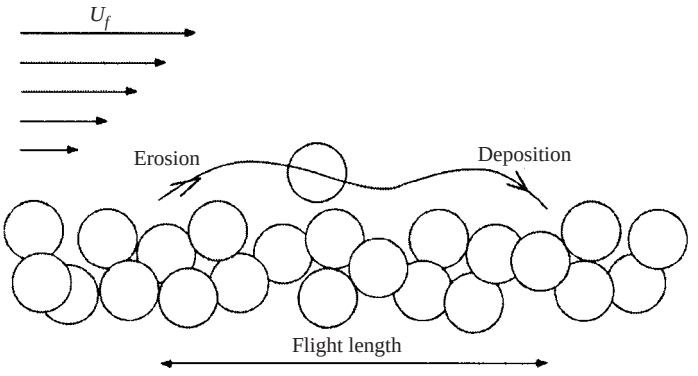

FIGURE 15. Sketch of a bed of particles sheared by a fluid flow.

4. Theoretical models

To account for our principal experimental observations, we propose two models for the surface density of moving particles, N_p: an erosion–deposition model and a kinematic trapping model, the former to account for the saturated states, and the latter to account for the slow decrease of the number of moving particles.

4.1. *An erosion–deposition model*

Let us consider a bed of particles sheared by a fluid flow (figure 15). The variation of the number N_p of moving particles per unit area is the result of two opposite processes occurring at the bed surface: erosion and deposition. Let $\dot{n}_e$ and $\dot{n}_d$ be the rates of erosion and deposition per unit area, respectively. The total variation rate of N_p, assuming spatial homogeneity, can then be written as

$$\frac{\mathrm{d}N_p}{\mathrm{d}t} = -\dot{n}_d + \dot{n}_e. \tag{11}$$

The deposition rate $\dot{n}_d$ can be modelled by considering that during one flight duration τ_p, N_p particles can be expected to stop per unit area. Moreover, since gravity is responsible for the deposition, the flight duration can be assumed to be proportional to the settling time d/V_S. Hence, the deposition rate can be expressed as

$$\dot{n}_d = \frac{N_p}{\tau_p}, \quad \text{with} \quad \tau_p = a\,\frac{d}{V_S}. \tag{12}$$

From the previously determined flight duration τ_p, the coefficient a can be taken as constant and equal to 15, according to equation (6).

The erosion of a particle, on the other hand, depends on the hydrodynamic force acting on it, i.e. it must involve the shear rate γ as the time scale. Moreover, erosion is likely to depend weakly on the number of moving particles, at least when this number is not too large. Thus, at first order, the erosion rate can be written as

$$\dot{n}_e = b\,\frac{\gamma - \gamma_t}{d^2} = 18b\,(\theta - \theta_t)\,\frac{V_S}{d^3}. \tag{13}$$

The coefficient b may depend weakly on the particle Reynolds number and on the number of moving particles, but here it is taken as a constant for the sake of simplicity. θ_t is the threshold for particle motion at time t, which depends on the surface microstructure of the bed. In our experiments, it increases from $\theta_{t,0} = 0.04$, when the flow is set up by resuspension, up to $\theta_{t,sat} = 0.12$ when the asymptotic state

is reached. The constant b can be determined from the flow rate measurements as follows. Equation (11) has the steady-state (or saturated) solution $\dot{n}_d = \dot{n}_e$, which with $\theta_t = \theta_{t,sat}$ and equations (12) and (13) leads to

$$N_{p,sat} d^2 = 18ab(\theta - \theta_{t,sat}). \tag{14}$$

This equation predicts that the number of moving particles increases linearly with the distance to the threshold $\theta_{t,sat}$, in agreement with the experimental law (10). Using the constants determined from the experiments, in particular $a = 15$ from (6) and $18ab = 0.47$ from (10), yields $b = 0.0017$. The linearity of (14) supports the modelling of the deposition and erosion rates based on the settling time and the shear rate.

Equation (11) should not only predict the saturated state, but also the preceding transient states. Since the experiments have shown that the armouring time is much greater than the hydrodynamic time scales, it can be considered that at any time the bed is in a quasi-equilibrium state, for which erosion just compensates deposition. The armouring itself might be imbedded in the threshold θ_t. Thus, the quasi-equilibrium solution of $\dot{n}_d = \dot{n}_e$, with initial threshold $\theta_t = \theta_{t,0}$, should yield the initial number of moving particles $N_{p,0}$. This conjecture leads to $N_{p,0} d^2 = 18ab\,(\theta - \theta_{t,0})$ and thus

$$\frac{N_{p,0}}{N_{p,sat}} = \frac{\theta - \theta_{t,0}}{\theta - \theta_{t,sat}}. \tag{15}$$

For $\theta = 0.15$, this equation predicts $N_{p,0}/N_{p,sat} = 3.7$ whereas the direct measurements yield 12. For $\theta = 0.24$, it predicts $N_{p,0}/N_{p,sat} = 2.5$ and the measurements 7. Thus, (15) successfully predicts $N_{p,0}$ to be higher than $N_{p,sat}$, but it underestimates $N_{p,0}$ by a factor of about three. Considering the crudeness of the hypotheses (in particular $b =$ constant), this discrepancy is not really surprising. Most importantly, this prediction supports the idea that the temporal evolution of the number of moving particles may be accounted for through the evolution of the threshold θ_t for particle motion. Following this idea, the erosion–deposition model could be amended by introducing a time-dependence of the threshold shear rate γ_t. However, a detailed description of the surface microstructure of the bed is still lacking for a convincing modelling of γ_t to be proposed. (As explained previously, the resolution of our ultrasonic probe was not high enough for such a description to be gained.) Instead, another way was preferred for accounting for this decrease, which is developed in the next section.

4.2. *A kinematic trapping model*

To account for the slow decrease of the surface density of the moving particles, and following the observation that this decrease is related to particles stopping in little crevices at the bed surface, we consider here explicitly the surface microstructure of the bed by modelling it as a flat surface with troughs in which moving particles may be trapped.

Consider a horizontal surface on which troughs, of typical size d, are randomly distributed (figure 16). The initial number of troughs per unit area is $N_{t,0}$ and the mean distance between the uniformly distributed troughs is $1/\sqrt{N_{t,0}}$. On this surface, particles are assumed to move uniformly with velocity U_p in the x-direction and may fall into the troughs. Initially the number of particles per unit area is $N_{p,0}$ and the mean distance between the particles is $1/\sqrt{N_{p,0}}$. A particle passing over a trough has the probability p of being trapped (the physical significance of this probability will appear below). A trough can trap one particle at most. How then does the number of moving particles decrease?

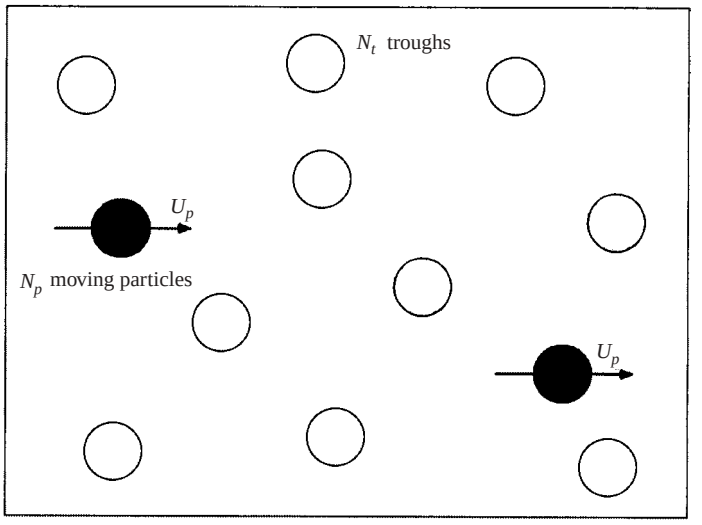

FIGURE 16. Sketch of the bed of particles for the trapping model. The numbers of moving particles and troughs per unit area are N_p and N_t, respectively.

Introducing the particle diameter d as the length scale, the above problem depends on the following three dimensionless parameters: (i) the fraction of the surface occupied by the particles at the initial time, $N_{p,0}d^2$, (ii) the ratio of the initial numbers of particles and troughs,

$$r = \frac{N_{p,0}}{N_{t,0}}, \tag{16}$$

and (iii) the trapping probability, p.

At time t, the number of troughs is $N_t(t) = N_{t,0} - N_{p,0} + N_p(t)$, and a characteristic distance between troughs is $1/\sqrt{N_t(t)}$. During time interval $\mathrm{d}t$, a particle travels over the distance $U_p\,\mathrm{d}t$, and sweeps the area $U_p\,\mathrm{d}t\,d$; it meets $N_t U_p\,\mathrm{d}t\,d$ troughs on average if the troughs remain uniformly distributed. Thus, during the time interval $\mathrm{d}t$, the probability for a particle to be trapped is $\mathrm{d}t/\tau(t)$, where $\tau(t) = 1/(pN_tU_pd)$ is the characteristic trapping time at time t. The mean number of trapped particles per unit area during $\mathrm{d}t$ is then $-\mathrm{d}N_p = N_p\,\mathrm{d}t/\tau$, whence the differential equation

$$\frac{\mathrm{d}N_p}{\mathrm{d}t} = -\frac{N_p}{\tau} = -p\,N_p\,U_p\,d\,(N_{t,0} - N_{p,0} + N_p). \tag{17}$$

Introducing the characteristic trapping time $\tau_0 = 1/(pN_{t,0}U_pd)$ at the initial time, this equation becomes, for the relative number of moving particles $N_p^* = N_p/N_{p,0}$ as a function of the dimensionless time $t^* = t/\tau_0$,

$$\frac{\mathrm{d}N_p^*}{\mathrm{d}t^*} = -N_p^*(1 - r + r\,N_p^*). \tag{18}$$

The solution of the above equation only depends on the initial ratio of particles to troughs, r. For $r = 1$, the solution is the algebraic decrease

$$N_p^*(t^*) = \frac{1}{1 + t^*}. \tag{19}$$

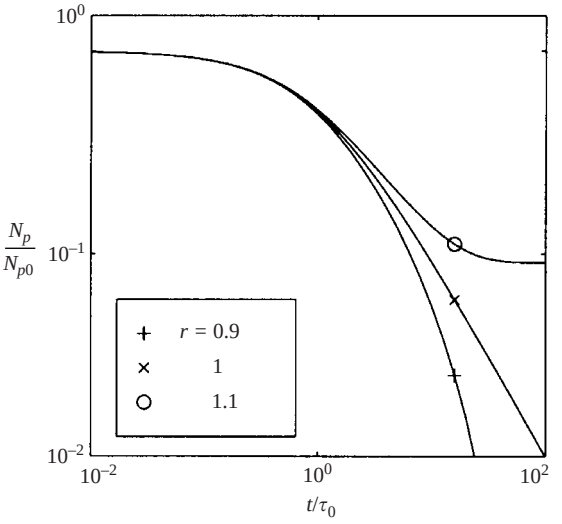

FIGURE 17. Temporal evolution of the number of moving particles $N_p/N_{p,0}$ according to the model (17) for $r = 0.9, 1, 1.1$.

For $r \neq 1$, the solution is

$$N_p^*(t^*) = \frac{(1-r)\mathrm{e}^{-(1-r)t^*}}{1 - r\,\mathrm{e}^{-(1-r)t^*}}. \tag{20}$$

For $r < 1$ (i.e. fewer particles than troughs), N_p^* tends to zero for large t^*. For $r > 1$ (i.e. more particles than troughs), N_p^* tends to $1 - 1/r$ as it should.

Figure 17 displays typical solutions of (19) (for $r = 1$) and (20) (for $r < 1$ and $r > 1$). It can be seen that these solutions are at least in qualitative agreement with the experiments: the existence of a saturation threshold, and decay over several orders of magnitude of τ_0. Finally, the particle flow rate at time t can be deduced as $Q = U_p\, N_p(t) = U_p\, N_{p,0}\, N_p^*(t)$.

We can now relate the parameters of the model to those of the experiments to obtain quantitative comparisons. We make the following four assumptions:

1. The initial number of troughs $N_{t,0}$ depends only on the way the bed is prepared (in the experiments reported above, by sedimentation of the totally resuspended flow).

2. The uniform velocity U_p of the model is taken as the mean velocity measured in the experiments, $U_p = 0.1\,\gamma d$.

3. The ratio $r = N_{p,0}/N_{t,0}$ and the initial number of troughs $N_{t,0}$ can be related to the Shields number as follows. Consider the number $N_{p,sat}$ of moving particles at saturation. On the one hand, the experiments show that for $\theta < \theta_{t,sat}$ this number is zero, and that for $\theta > \theta_{t,sat}$ it is $N_{p,sat} d^2 = 0.47(\theta - \theta_{t,sat})$. On the other hand, the model predicts that for $r < 1$, $N_{p,sat}$ is zero, and for $r > 1$, $N_{p,sat} = N_{p,0} - N_{t,0} = N_{t,0}(r-1)$. Equating the two expressions for $N_{p,sat}$ gives

$$N_{t,0} d^2 (r-1) = 0.47(\theta - \theta_{t,sat}).$$

Extrapolating this relation down to the threshold $\theta_{t,0}$, for which r is zero, we obtain $N_{t,0} d^2 = 0.47\,(\theta_{t,sat} - \theta_{t,0})$. With $\theta_{t,0} = 0.04$ and $\theta_{t,sat} = 0.12$, we finally obtain $N_{t,0}$ and the relation between r and the Shields number:

$$N_{t,0} d^2 = 0.038, \tag{21}$$

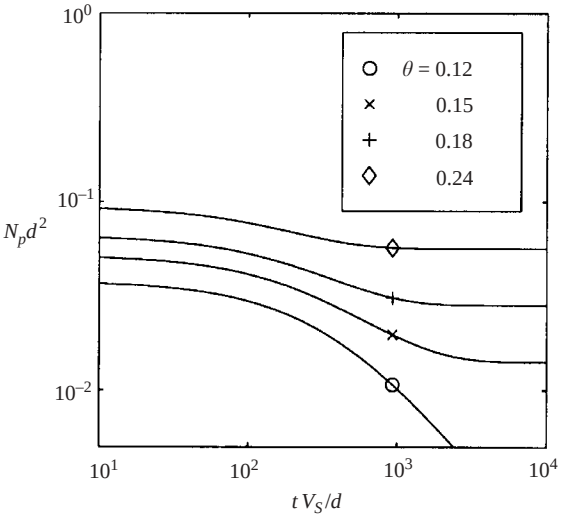

FIGURE 18. Temporal evolution of the surface density of the moving particles N_p according to the model (18) with the correlations (22) and (23), for $\theta = 0.12 \ldots 0.24$.

and

$$r = \frac{\theta - \theta_{t,0}}{\theta_{t,sat} - \theta_{t,0}}. \tag{22}$$

4. The trapping probability p is related to the time spent by a particle above a trough. Indeed, in order to be trapped, the particle has to force some fluid out of the trough. Thus, the trapping condition is that the time spent by the particle above the trough be greater than the drainage time. The order of magnitude of the first time is $d/U_p \sim 1/\gamma$, and the order of the latter is the settling time d/V_S. The ratio of these two times is equal to, dimensionally, the inverse Shields number. The simplest expression of the trapping probability is therefore $p \sim 1/\theta$. The constant coefficient in this law can be determined by considering that at the threshold for particle motion $\theta_{t,0}$, particles easily fall in troughs because their velocity is small, so that the trapping probability is the highest and equal to unity. Finally, this probability can be written as

$$p = \frac{\theta_{t,0}}{\theta} \quad \text{with} \quad \theta_{t,0} = 0.04. \tag{23}$$

Equations (21), (22) and (23) relate the three parameters of the model to those of the experiments. The trapping time τ_0 can now be estimated as

$$\tau_0 = \frac{1}{p\, N_{t,0}\, U_p\, d} \approx 370\, \frac{d}{V_S} \approx 100\,\text{s}. \tag{24}$$

Figure 18 diplays the temporal evolution of the number of moving particles $N_p(t)d^2 = r\, N_{t,0} d^2\, N_p^*(t/\tau_0)$, with $N_p^*(t/\tau_0)$, $N_{t,0}d^2$, r and τ_0 given by (20), (21), (22) and (24), respectively. This figure shows that the trapping model exhibits temporal evolution of the number of moving particles similar to the experimental evolution shown in figure 13. In particular, the model yields saturation times $t_{sat} \approx 10^3 d/V_S$, much greater that the hydrodynamic time scales d/V_S and $1/\gamma$. However, this saturation time remains smaller than the observed time by a factor 20 to 100.

The above trapping model, through the modelling of surface phenomena, predicts the right trends, specifically the correct sense of the temporal evolution of the number

of moving particles, the correct dependence of the saturated state as a function of the Shields number, and saturation times much higher than the hydrodynamic time scales (although still too small). Of course the model might easily be amended in order to reproduce greater saturation times. This could be done, for example, by refining the trapping probability, or by taking into account erosion, or by introducing more dynamic rules for the filling of the troughs. However, without additional information from experiments, such modifications would be unjustified, and are merely as *ad hoc* hypotheses. The main problem at this point is still the lack of experiments offering a description of the surface microstructure of sheared granular beds.

5. Summary and discussion

As mentioned in the introduction, improvements in the modelling of the transport of particles on a bed by a shear flow require a detailed knowledge of the motion of individual particles within the moving layer. This also raises the question of properly assessing the slow temporal evolution associated with bed armouring, and consequently the way by which stationary transport is achieved. Ways that can be envisioned are bed vibration or mechanical compaction; a more practically relevant way, however, is compaction by the fluid shear itself, by which the state of compaction is linked to the strength of the shear.

Of particular interest are the surface density of the moving particles, their velocity, and the length and duration of the saltation jumps, or flights, of the particles as they lift off the bed. We determined such quantities for viscous flows from measurements in an annular channel for an initially loosely packed bed, and give not only their mean values but also their distributions, in both the transient and the saturated states, and the associated time scales. In order to help understand the experimental results, two models have been proposed, one for the stationary erosion and deposition processes, and the other for the transient evolution.

The first evidence of the slow temporal evolution is given by the decrease of the bed surface height as measured by ultrasonic probes. For a relatively low Shields number of 0.17, the bed thickness decreases strongly over about two days, and then appears to reach a constant value. The transient time scale is several orders of magnitude larger than the two hydrodynamic time scales, i.e. the inverse shear rate and the settling time. The reason for the observed bed-thickness decrease can be attributed to the rearrangement of the bed microstructure, predominantly near the bed surface. The rearrangement in turn is responsible for 'bed armouring' and affects the threshold for particle motion and the transport rate. The threshold increases from $\theta_{t,0} = 0.04$, which corresponds to a settled bed after total resuspension, to $\theta_{t,sat} = 0.12$ when the bed has reached its saturated state. This value is the range of those found by White (1970), Mantz (1978) and Yalin & Karahan (1979).† The saturated threshold therefore seems to be independent of the way the bed is prepared. Although bed armouring is a well-known phenomenon (Chin *et al.* 1994; Raudkivi 1998), it is believed to occur with non-uniform sediment size only. Our experiments show that it can also occur with nearly uniform particle size.

For the explored Shields number range ($\theta < 0.24$), particles were observed to mainly roll and slide on the underlying bed, with small saltation flights in between which they stop for a while in little crevices. No clear distinction was found possible between the

† For $\theta = 0.12$, the particle Reynolds number (4) is equal to 0.15, which corresponds to a particle Reynolds number based on the friction velocity equal to $\sqrt{0.15} = 0.39$.

crawling (rolling and sliding) and saltating motions; due to the geometrical disorder of the bed, the moving particles easily lift off as they leave a local protrusion, and fly distances of a few particle diameters. The most probable flight length, L, is independant of time but increases with Shields number: it is about one diameter when close to threshold Shields numbers, and up to five diameters at four times this threshold. These flights can be attributed to the fact that, for viscous flow, the advection time of the particle, i.e. the time needed to travel over one diameter, is shorter than the drainage time needed for the falling particle to force out the fluid below it. The flight durations were also measured, revealing distributions with well-defined peaks at about 15 times the settling time d/V_S. These flight durations were found to not vary significantly with time and shear rate. Although only one system of fluid and particles has been used in our experiments, this result can be expected to be more general, since the underlying idea — also used in the erosion–deposition model — is that particle deposition is controlled mainly by gravity. The lift force may also be involved in the flight duration, but, in our study, this force is probably negligible compared to the apparent weight of the particle: King & Leighton (1997) showed that for a particle rolling and sliding on a plane wall, the shear stress needed to lift up the particle corresponds to Shields numbers about 10, much higher than ours.

The lift-off is likely to be due to the geometrical disorder of the bed surface, each local protrusion playing the role of a little 'ramp', and it cannot be attributed to elastic rebounds. Indeed, it has been shown that even if a solid particle falling in a liquid may rebound on a solid surface, the condition for a non-zero coefficient of rebound is that the Stokes number of the particle, which measures the ratio of particle inertia and viscous forces, must be greater than 20 (Gondret *et al.* 1999). In our experiments, this number was at least one order of magnitude lower, so that particles cannot rebound. Particles were also observed to have significant rotation, and this rotation probably has a significant effect on the motion. Deeper insight into this question could be gained from experiments on a single moving particle on a fixed bed, as done by Francis (1973), and from numerical investigation of the motion of a particle near a rough bed, including particle rotation (existing numerical simulations of particle trajectories, such as that performed by Sekine & Kikkawa (1992), ignore rotation). Finally, it can be noted that the flight lengths found in this study are smaller than those found in turbulent water flows, i.e. for much higher particle Reynolds numbers: Fernandez Luque & van Beek (1976) found $L/d \approx 16$, which was constant in the explored Shields number range. This disagrees with the experiments reported in Sekine & Kikkawa (1992), which show L/d increasing strongly with Shields number from a few tens up to three hundred. Note that the numerical calculations of Sekine & Kikkawa (1992) reproduce these long jumps using a coefficient of rebound of 0.65, which, considering Gondret *et al.* (1999), appears very high for particles with diameter less than one millimetre.

Coming back to our results, the mean particle velocity, U_p, was found to be independent of the transient evolution, i.e. of the state of bed compaction, and equal to $0.10\,\gamma d$, i.e. proportional to the shear rate. The numerical coefficient decreases only slighly, by about 10%, when doubling the shear rate. Time series of particle velocities exhibit peaks at about four times this mean velocity, which correspond to the longer flight lengths. The velocity distributions, moreover, decay monotically, close to exponential, with many slow and few fast velocities which correspond to short and long flight lengths, respectively. Again, from these distributions, no distinction was found possible between crawling and saltating particles.

The proportionality of U_p to the shear rate, i.e. to the shear stress, contrasts with the viscous resuspension theory by Leighton & Acrivos (1986), which predicts a quadratic dependence. It also contrasts with the experimental results by Fernandez Luque & van Beek (1976) for turbulent flows on erodible beds. They found $U_p = 11.6\,(u^* - 0.7u_t^*)$, where u^* and u_t^* are the friction velocity and the threshold friction velocity, respectively, i.e. that the particle velocity is proportional to the square root of the shear stress.

In addition to particle velocities, the surface density of moving particles, N_p, was also investigated. We found that, contrary to the particle velocities, it decreases slowly with time by one order of magnitude, over the same long time scales as the bed thickness. It can thus be concluded that bed armouring due to fluid shear affects the bed thickness, the threshold for particle motion and the surface density, over the same time scales.

At saturation, the surface density $N_{p,sat}$ of the moving particles was found to increase linearly with the distance to the threshold, $N_{p,sat}d^2 = 0.47(\theta - \theta_{t,sat})$. This linear dependence is in agreement with several turbulent-flow studies, although our coefficient is lower. In the experiments by Fernandez Luque & van Beek (1976), the surface density was determined from visual observation, and found to be $N_p d^2 = 1.8(\theta - \theta_t)$ for $\theta - \theta_t < 0.1$. In numerical studies, the linear law for N_p arises as a consequence of Bagnold's hypothesis, according to which the thickness of the moving layer corresponds to the fluid shear stress at the bed reduced to θ_t (Bagnold 1956).† In particular, Sekine & Kikkawa (1992) found $N_p d^2 = 2.4(\theta - \theta_t)$. From an heuristic model for ripple formation, Andersen (2001) also found such a linear law, with the coefficient equal to 2.9.

As a consequence of the laws for the surface density and particle velocity, the saturated flow rate $Q_{sat} = N_{p,sat}U_p$ is a quadratic function of the Shields number, $Q_{sat}d^2/V_S = 0.85\,\theta\,(\theta - \theta_{t,sat})$. This result is different from the predictions of the two available models for viscous flow, those of Bagnold (1956) and Leighton & Acrivos (1986). (Less surprisingly, this result is also different from the classical semi-empirical laws which all predict dimensionless flow rates close to $(\theta - \theta_t)^{3/2}$, (see Wiberg & Smith 1989) among others). Although these two viscous-flow models are significantly different – in particular Leighton & Acrivos (1986) ignores particle inertia – both consider that the vertical profiles of velocity and concentration correspond to an equilibrium between settling and a dispersive effect due to particle interactions. Both models predict that the particle flow rate scales as the shear rate to the power three, whereas our results show a quadratic dependence. Basically, the cubic law arises because the thickness of the moving layer increases linearly with the shear rate, so that the mean velocity scales as the square of the shear rate, not linearly as in our experiments.

In order to better understand the underlying mechanisms governing the experimental observations, two models were developed, a 'dynamic' one and a 'kinematic'

† However, a different power law, with an exponent of 3/2, was obtained by van Rijn (1984). From his particle-velocity calculations combined with the analysis of many flow rate measurements, one can deduce from his equations (14) and (22)

$$N_p d^2 = (0.068/D_*^{0.3})\,[(\theta - \theta_t/\theta_t)]^{1.5},$$

where $D_* = d\,((\rho_p/\rho_f - 1)g/(\mu/\rho_f)^2)^{1/3}$ is a dimensionless particle diameter.

one. The dynamic model aims at understanding the linear relationship between the saturated surface density of moving particles and the Shields number. Based on the mass conservation equation (11) of the moving particles, it requires the modelling of the deposition and erosion rates. The basic assumption for the deposition rate $\dot{n}_d$ is that its time scale is governed by gravity and not by the shear rate, so that $\dot{n}_d$ can be taken to be equal to N_p/τ_p, where τ_p is the characteristic flight duration evaluated by the experiments to be 15 times the settling time d/V_S. The erosion rate, on the other hand, was assumed to be dependent on the hydrodynamic force, i.e. proportional to the shear rate or more precisely to $(\gamma - \gamma_t)/d^2$ at the dominant order, where γ_t is a threshold shear rate. At equilibrium (equal deposition and erosion rates), this model predicts that the saturated surface density $N_{p,sat}$ (which corresponds to $\gamma_t = \gamma_{t,sat}$) is proportional to $\theta - \theta_{t,sat}$, in agreement with the experiments. This confirms that the deposition and erosion rates are essentially controlled by the settling time and shear rate, respectively.

The above model should also yield the slow decay of the number of moving particles, if the slow increase of the shear-rate threshold is taken into account. We have shown that this idea does not lead to close agreement with the experiments, in all likelihood because of the first-order shear-rate dependence. A higher-order modelling has not been attempted as the experimental data set does not allow it.

Instead, since the observed slow evolution of the bed thickness, threshold shear rate and number of moving particles was attributed to the bed armouring, it was modelled at first order as a surface phenomenon through a trapping model. This has been done by considering the bed as a flat surface with troughs in which the moving particles may be trapped, which is consistent with the observation that particles may stop in little crevices. Apart from the particle velocity and diameter which define the time and length scales, this kinematic model (which ignores explicit consideration of the fluid flow) involves three additional parameters: the initial numbers of troughs and moving particles, and a trapping probability for a particle to actually be held in a trough when passing over it. These parameters have been set in order to fit the measured saturated flow rates, and not the transient stages. The resulting time variations of the particle flow rate predicted by this model qualitatively reproduce those observed in the experiments. In particular, the model predicts saturation times several hundred times higher than the hydrodynamic time scales. However, it still underestimates the initial flow rates by a factor 3 to 5, and also underestimates the saturation times by a factor 20 to 100. The model might easily be amended in order to reduce this gap, in particular by introducing erosion or refining the trapping probability. However, implementing such refinements would only improve the surface model, while still neglecting what happens below the surface, which is likely to correspond to corrections of the same order. More experimental work is needed first in order gain a better knowledge of the surface and sub-surface structures of the bed at the scale of one particle diameter, and its evolution with time.

Finally, it must be noted that the number of moving particles displayed an intermittent character, both in space and time, which is responsible for the major part of the scatter of our measurements. This probably also occurs for higher particle Reynolds number in water flows, and does not seem to have been considered in previous studies. A precise study of this intermittency remains to be done.

We thank E. J. Hinch and F. Risso for valuable ideas and suggestions, as well as G. Imbert, I. Altuna Urquia and E. Larrieu for their help in the experiments.

REFERENCES

Andersen, K. H. 2001 A particle model of rolling grain ripples under waves. *Phys. Fluids* **13**, 58–64.

ASCE Task Committee on Flow and Transport over Dunes 2002 Flow and transport over dunes. *J. Hydraul. Engng* **128**, 726–728.

Bagnold, R. A. 1956 The flow of cohesionless grains in fluids. *Phil. Trans. R. Soc. Lond.* A **249**, 235–297.

Bagnold, R. A. 1966 An approach to the sediment transport problem from general physics. *US Geol. Surv. Prof. Paper* **422-I**, 1–37.

Bagnold, R. A. 1973 The nature of saltation and of 'bed-load' transport in water. *Proc. R. Soc. Lond.* A **332**, 473–504.

Blondeaux, P. 1990 Sand ripples under sea waves. Part 1. Ripple formation. *J. Fluid Mech.* **218**, 1–17.

Blondeaux, P. 2001 Mechanics of coastal forms. *Annu. Rev. Fluid Mech.* **33**, 339–370.

Buffington, J. M. & Montgomery, D. R. 1997 A systematic analysis of eight decades of incipient motion studies, with special reference to gravel-bedded rivers. *Water Resour. Res.* **33**, 1993–2029.

Campbell, C. S. 1990 Rapid granular flows. *Annu. Rev. Fluid Mech.* **22**, 57–92.

Charru, F. & Mouilleron-Arnould, H. 2002 Instability of a bed of particles sheared by a viscous flow. *J. Fluid Mech.* **452**, 303–323.

Chin, C. O., Melville, B. W. & Raudkivi, A. J. 1994 Streambed armoring. *J. Hydraul. Engng* **120**, 899–918.

Einstein, H. A. 1950 The bedload function for sediment transportation in open channel flow. *Tech. Bull.* 1026. US Dept of Agriculture, Washington DC, pp. 1–71.

Engelund, F. & Fredsoe, J. 1976 A sediment transport model for straight alluvial channels. *Nordic Hydrol.* **7**, 293–306.

Fernandez Luque, R. & van Beek, R. 1976 Erosion and transport of bedload sediment. *J. Hydraul. Res.* **14**, 127–144.

Francis, J. R. D. 1973 Experiments on the motion of solitary grains along the bed of a water stream. *Proc. R. Soc. Lond.* A **332**, 443–471.

Gondret, P., Hallouin, E., Lance, M. & Petit, L. 1999 Experiments on the motion of a solid sphere toward a wall: From viscous dissipation to elastohydrodynamic bouncing. *Phys. Fluids* **11**, 2803–2805.

Kadanoff, L. P. 1999 Built opon sand: Theoretical ideas inspired by granular flows. *Rev. Mod. Phys.* **71**, 435–444.

King, M. R. & Leighton, D. T. 1997 Measurement of the inertial lift on a moving sphere in contact with a plane wall in a shear flow. *Phys. Fluids* **9**, 1248–1255.

Leighton, D. & Acrivos, A. 1986 Viscous resuspension. *Chem. Engng Sci.* **41**, 1377–1384.

Mantz, P. A. 1978 Bedforms produced by fine, cohesionless, granular and flakey sediments under subcritical water flows. *Sedimentology* **25**, 83–103.

Meland, N. & Norrman, J. O. 1966 Transport velocities of single particles in bed-load motion. *Geogr. Ann.* **48A**, 165–182.

Mouilleron-Arnould, H. 2002 Instabilités d'un milieu granulaire cisaillé par un fluide. Thèse de Doctorat, Université Paul Sabatier, Toulouse, France.

Raudkivi, A. J. 1998 *Loose Boundary Hydraulics.* A. A. Balkema, Rotterdam.

Richards, K. J. 1980 The formation of ripples and dunes on an erodible bed. *J. Fluid Mech.* **99**, 597–618.

van Rijn, L. C. 1984 Sediment transport, part I: bed load transport. *J. Hydraul. Engng* **110**, 1431–1456.

Sekine, M. & Kikkawa, H. 1992 Mechanics of saltating grains. II. *J. Hydraul. Engng* **118**, 536–558.

White, S. J. 1970 Plane bed thresholds of fine grained sediments. *Nature* **228**, 152–153.

Wiberg, P. L. & Smith, J. D. 1989 Model for calculating bed load transport of sediment. *J. Hydraul. Engng* **115**, 101–123.

Yalin, M. S. & Karahan, E. 1979 Inception of sediment transport. *J. Hydr. Div., ASCE* **105**, 1433–1443.